Article:
Toll, V., Rahu, J., Keernik, H. et al. (2024) Glaciation of liquid clouds, snowfall, and reduced cloud cover at industrial aerosol hot spots. Science, 386 (6723). pp. 756-762. ISSN: 0036-8075

https://doi.org/10.1126/science.adl0303

Title: Glaciation of liquid clouds, snowfall and reduced cloud cover at industrial aerosol hot spots

Authors: Velle Toll[1]*, Jorma Rahu[1], Hannes Keernik[1], Heido Trofimov[1], Tanel Voormansik[1], Peter Manshausen[2], Emma Hung[3], Daniel Michelson[3], Matthew W. Christensen[4], Piia Post[1], Heikki Junninen[1], Benjamin J. Murray[5], Ulrike Lohmann[6], Duncan Watson-Parris[7], Philip Stier[2], Norman Donaldson[3], Trude Storelvmo[8], Markku Kulmala[9], Nicolas Bellouin[10]

Affiliations:

[1]Institute of Physics, University of Tartu; Tartu, Estonia.

[2]Department of Physics, University of Oxford; Oxford, UK.

[3]Environment and Climate Change Canada; Toronto, Canada.

[4]Atmospheric Science & Global Change Division, Pacific Northwest National Laboratory; Richland, Washington, USA.

[5]Institute for Climate and Atmospheric Science, School of Earth and Environment, University of Leeds; Leeds, UK.

[6]Institute of Atmospheric and Climate Science, ETH Zürich; Zürich, Switzerland.

[7]Scripps Institution of Oceanography and Halıcıoğlu Data Science Institute, University of California San Diego, USA.

[8]Department of Geosciences, University of Oslo; Oslo, Norway.

[9]Institute for Atmospheric and Earth System Research, University of Helsinki; Helsinki, Finland.

[10]Department of Meteorology, University of Reading; Reading, UK.

*Corresponding author. Email: velle.toll@ut.ee

Abstract: The ability of anthropogenic aerosols to freeze supercooled cloud droplets remains debated. Here, we present observational evidence for the glaciation of supercooled liquid-water clouds at industrial aerosol hot spots at temperatures between -10 and -24 °C. Compared to the nearby liquid-water clouds, the shortwave reflectance is reduced by 14% and longwave radiance increased by 4% in the glaciation-affected regions. There is an 8% reduction in cloud cover and an 18% reduction in cloud optical thickness. Additionally, daily glaciation-induced snowfall accumulations reach 15 mm. Glaciation events downwind industrial aerosol hot spots indicate that anthropogenic aerosols likely serve as ice-nucleating particles. However, rare glaciation events downwind of nuclear power plants indicate that factors other than aerosol emissions may also play a role in the observed glaciation events.

One-Sentence Summary: Supercooled cloud droplets transformed into ice crystals downwind strong anthropogenic air pollution sources.

Main Text: It remains uncertain to what extent anthropogenic aerosols, i.e. tiny air pollution particles, counteract global warming induced by anthropogenic greenhouse gases (*1*, *2*). Moreover, it remains unclear if, in addition to serving as cloud condensation nuclei (CCN), anthropogenic aerosols impact clouds and climate by serving as ice nucleating particles (INPs) (*3*-16). Supercooled liquid-water clouds exist in the Earth's atmosphere because INPs are required for ice nucleation at higher subzero temperatures than about -36 °C, but INPs are a rare subset of atmospheric aerosols (*3*).

Anthropogenic INPs have been suggested as one of the multiple possible reasons for the observed plume-shaped areas of anthropogenic snowfall downwind of industrial facilities (*17*–*20*). Such industrial facilities emit heat, water vapour, aerosol precursor gases and aerosol particles that could serve as CCN or INPs. Plume-shaped areas of snow downwind industrial facilities have been suggested to result directly from condensation cloud formed from the water vapour emitted by industry (*18*, *19*), due to the interaction of industrial emissions with supercooled fog below the stacks (*17*, *20*, *21*), from a seeder-feeder process when naturally occurring snow acts as seed for further snow in the industrial condensation cloud below (*22*) and from the impact of anthropogenic emissions on the cloud deck above (*18*). Here, we rely on remote sensing to study the impact of industrial emissions on the supercooled cloud decks above the stacks and identify which industrial sources lead to glaciation (detailed methods under supplementary Materials and Methods). We observe the glaciation of supercooled liquid-water clouds downwind of 67 anthropogenic aerosol hot spots, indicating that various industrial aerosols serve as INPs. At four sites, we also see glaciation downwind of nuclear power plants likely emitting little to no aerosols serving as INPs, indicating that factors other than INPs may also play a role in the observed glaciation events. However, it is also possible that buoyant plumes from the nuclear power plants loft nearby aerosols that serve as INPs.

Glaciation of liquid-water clouds at anthropogenic aerosol hot spots

We discovered glaciation events where supercooled liquid-phase clouds are converted into ice clouds near anthropogenic aerosol hot spots like metallurgical and cement industries, coal-fired power plants and oil refineries (Fig 1, S1, Movies S1 and S2) and, in five cases, downwind nuclear power plants (Fig S2). We identified 67 different aerosol sources leading to glaciation events (Table 1, Fig 2a, supplementary methods “Identification of glaciation events”) and 298 glaciation events at five aerosol sources studied in more detail over the years 2000 to 2021 (supplementary methods “Analysis of MODIS satellite data for selected aerosol sources”). To identify glaciation events, we detected plume-shaped areas of reduced cloud cover in the near-infrared composite satellite images from the Moderate Resolution Imaging Spectroradiometer (MODIS) instrument on board the Terra satellite. To identify the aerosol sources leading to glaciation, we used Google Maps. Using the National Aeronautics and Space Administration (NASA) Worldview interactive interface, we hand-logged the glaciation-affected regions at five aerosol sources for more detailed analysis.

Overlays of satellite data from polar-orbiting Terra MODIS and Geostationary Operational Environmental Satellite (GOES) Advanced Baseline Imager (ABI) with ground-based precipitation radar data reveal a causal sequence from glaciation to snowfall to reduced cloud cover (example in Movie S2). We infer the likely physical explanation for glaciation events (Fig 3) based on cloud perturbations at various aerosol sources and various products from remote

sensing instruments (examples in Fig 1). In MODIS and GOES ABI data, we see ice clouds in the middle of the supercooled liquid-water cloud decks downwind of industrial aerosol sources (Fig 1a). We see snowfall in ground-based precipitation radar data (Fig 1b, S3 to S5, Movies S2 and S3), which is likely induced by the growth of ice crystals at the expense of supercooled cloud droplets because of the lower saturation pressure of water vapour over ice than over liquid water (*23*). And finally, we see reduced cloud cover in MODIS and GOES ABI data (Fig 1c, S1). At the same time, the plume-shaped areas of ice clouds, snowfall and reduced cloud cover overlap strikingly well (Fig S5, Movie S2).

Passive and active remote sensing of clouds and precipitation reveal both ice clouds in the middle of supercooled liquid-water clouds (Fig 1a) and glaciation-induced snowfall (Fig 1b). The glaciation-induced cloud perturbations identified in satellite data remain visible for 17 hours in GOES ABI images (supplementary methods "Analysis of GOES ABI satellite data") and glaciation-induced snowfall events identified in ground-based precipitation radar data for 8 hours on average (supplementary methods "Analysis of ground-based precipitation radar data"). While the glaciation-induced cloud perturbations cover 4066 km^2, the plume-shaped areas of snow cover 2161 km^2 on average. Even though glaciation itself happens quickly and night-time identification of cloud phase from passive remote sensing is challenging (*24*), we identify ice clouds in the middle of supercooled liquid-water clouds in 69% of the cases studied using geostationary satellite data (supplementary methods "Analysis of GOES ABI satellite data"). Moreover, we observe plume-shaped snowfall areas in 29% of the studied cases where we have precipitation radar data available. For all the precipitating cases where we have dual-polarimetric radar data available, the hydrometeor classification identifies the type of precipitation as snow. Interestingly, in three cases, plume-shaped areas with fresh snow on the ground are seen in satellite data after the clouds have cleared away (example in Fig 1d). The glaciation-induced snowfall significantly affects precipitation amounts close to the studied industrial aerosol sources. Daily snowfall accumulations due to glaciation events reach 15 mm, while snowfall intensity is 1.2 mm/h on average (see supplementary methods "Analysis of ground-based precipitation radar data").

Linking glaciation events to industrial emissions

Most of the identified glaciation events occur downwind of strong localised anthropogenic aerosol sources (Table 1). The cloud perturbations associated with glaciation events have a similar shape and spatial extent to CCN-polluted cloud tracks in liquid-water clouds (Fig S6; *25*, *26*). Both CCN perturbations on clouds and glaciation events have a characteristic head pointing towards the industrial point source, or the perturbation area is plume-shaped, indicating that the industrial source is inducing the observed cloud perturbation (Figs 1, S1 to S6). The widths of plume-shaped CCN perturbations on clouds and glaciation events are tens of kilometres and the lengths are hundreds of kilometres (Fig S6). Glaciation events occur under similar but colder meteorological conditions than CCN perturbations (Figs 4a and 4b, S7 to S9; *27–29*). Glaciation events are more frequent in colder months (November to February; Figs S10 and S11). Visual classification of cloud types indicates that both CCN perturbations and glaciation events occur in stratiform clouds (*26*; Fig 1, S1, S6). Based on atmospheric reanalysis and MODIS satellite data, glaciation events are seen more likely in high pressure situations with uniform stratiform cloud decks, high cloud fraction, average cloud water path around 184 g/m^2, low relative humidity above clouds and a statically stable lower troposphere (Figs 4b, S7 and S8; supplementary

methods “Meteorological conditions favourable for glaciation events”). Such meteorological conditions have previously been found to be favourable for the occurrence of stratiform clouds susceptible to aerosols and for the formation of aerosol-induced cloud perturbations visible in MODIS satellite images (*28*). In addition, the plume-shaped glaciation events studied here are visually distinct from the oval-shaped aircraft-induced hole punch and canal clouds (Fig S6) and form under higher subzero temperatures compared to the hole punch clouds (Fig 4a). MODIS cloud top temperatures show that glaciation events occur mostly at temperatures between -10 to -24 °C (Fig 4a), but the characteristic cloud top temperatures vary depending on the aerosol source (Fig S9a). Downwind the cement plants in Volsk and Fokino, glaciation events occur at higher subzero temperatures compared to other sites (Figs S9a and S9b), but at Volsk and Fokino, the cloud top temperatures between about -15 °C and 0 °C are also in general more frequent in supercooled liquid-water cloud decks in winters (Fig S9c), where glaciation events mainly occur (Figs S10 and S11). At the temperatures characteristic of glaciation events, the adiabatic cooling down to homogeneous freezing temperatures is less likely compared to the conditions characteristic of the hole punch clouds at Moscow Domodedovo airport (Fig 4a) situated in Eastern Europe between the studied sites at Fokino and Cherepovets. However, hole punch clouds can also occur at higher subzero temperatures *(30, 31)*. Thus, it remains unclear how representative the cases are at the Moscow Domodedovo airport.

We link observed glaciation events to industrial point sources by modelling aerosol dispersion from point sources using Hybrid Single-Particle Lagrangian Integrated Trajectory (HYSPLIT) version 5 concentration plume model (*32*) (supplementary methods “Analysis of aerosol dispersion from point sources”). We compare simulated aerosol-polluted areas to the areas of cloud perturbations identified in MODIS satellite data, keeping in mind that the heat and water vapour from the pollution sources are dispersed within the same plumes. The aerosol dispersion plumes overlap exceptionally well with the areas of glaciation, snowfall and reduced cloud cover (Figs 4c and 4d). The difference in azimuth angles (the angle relative to the north) between the observed glaciation events and simulated aerosol-polluted areas downwind of industrial sites is less than 20° for 75% of cases (Fig 4d). Moreover, the shapes of simulated aerosol dispersion plumes are very similar to glaciation events and have distinctive heads pointing towards the pollution sources (example in Fig 4c).

We test if drivers other than aerosols could explain the observed glaciation events by looking for glaciation events downwind nuclear power plants. Nuclear power stations are sources of heat and water vapour, similarly to studied aerosol hot spots, but likely emit little to no aerosols serving as INPs. The heat from the studied aerosol hot spots causes buoyancy and vertical motions of air. The buoyancy-driven cooling of air could be linked to more efficient ice formation in mixed-phase clouds (*33*) and the clouds studied here could potentially be mixed-phase clouds already before they are impacted by aerosol pollution sources. Moreover, the emitted water vapour can cause supersaturation and lead to the formation of a condensation cloud. To cover the range of meteorological conditions favourable for glaciation, we chose 11 nuclear power stations close to the aerosol sources where we identified glaciation events in Eastern Europe (Fig 2a) and analysed supercooled clouds over the winters (December, January, February) 2005 to 2014. In agreement with previous observations of anthropogenic snowfall events at natural draft cooling towers (*18*), we observe glaciation downwind nuclear power stations in five cases (four stations) (Fig 2a, S2). Although glaciation events at nuclear power stations are relatively rare, the

existence of these events indicates that reasons other than aerosols serving as INPs may also play a role in the observed glaciation events. An alternative explanation could be that buoyant plumes from the nuclear power plants loft nearby aerosols that serve as INPs.

We observe anthropogenic glaciation of supercooled liquid-water clouds more frequently at specific aerosol sources like processing sites of metals and minerals, including cement production (Table 1). In fact, 78 % of identified aerosol sources leading to glaciation events fall under the categories of metals and minerals (Table 1). Aerosols from these sources are known to serve as INPs, as discussed in the next section. At the same time, CCN perturbations occur predominantly at sulphate-emitting aerosol sources (*26*). Cherepovets steel plant is known to frequently lead to anthropogenic CCN perturbations on clouds (*28*, *29*). At the Cherepovets steel plant, CCN-induced perturbations on clouds are eight times more frequent than glaciation events (Figs S12 and S13).

Which anthropogenic aerosols could nucleate ice at the studied air pollution sources?

We identified anthropogenic glaciation events at 67 industrial aerosol sources in North America, Europe and Asia (supplementary methods "Identification of glaciation events;" Table 1; Fig 2a). The 32 metallurgical plants are mining and processing sites of iron, copper, nickel, and alumina, together with the steel industry and machine building (Table 1). Metallic particles have been previously found in elemental, oxide, and sulfate forms in ice residues under both cirrus and mixed-phase cloud conditions (*34–36*). Out of 20 processing sites of minerals, 16 are cement plants. The remaining ones are factories producing asphalt, mineral fertilisers and other minerals. Various minerals are known to be effective INPs (*3*, *37–39*). The tectosilicates, including certain feldspars and quartz samples, have been shown to have much greater ice-nucleating activities than clay minerals (*40*). Laboratory experiments have also indicated that cement particles act as INPs (*41*). Cement is produced from calcium carbonates and contains other materials such as CaSO4 (gypsum or anhydrite). While calcium carbonates have been shown to have a relatively low ice nucleating activity, similar to that of the clay minerals (*40*), anhydrite has been implicated in the ice nucleating ability of both volcanic and combustion ashes (*42*, *43*). At three glaciation sites, paper and cellulose are produced, while again previous laboratory experiments support that cellulose particles act as INPs (*44*, *45*). In addition, lignin is also used in paper production and has been shown to be an effective ice nucleant (*46*).

Out of 12 hydrocarbon combustion sites identified to lead to glaciation events, 7 are coal-fired power plants and three are oil refineries. In addition, coal is used to produce thermal energy at multiple studied metallurgical and cement plants. It is important to note that oil and coal are not pure hydrocarbons but also contain minerals (*47*). Moreover, particles can be lofted during combustion, producing airborne ashes like coal fly ash. Laboratory experiments suggest that combustion ashes with various compositions and origins are effective INPs at temperatures below -12 °C (*14*, *43*). Moreover, fly ash from a power plant plume was found to serve as INPs by (*20*). The ability of combustion carbonaceous aerosols (soot) to serve as INPs at the temperatures of mixed-phase clouds is debated and recent laboratory experiments suggest that soot particles are not effective INPs (*3*, *11*, *12*).

More work is clearly needed to better understand the ice-nucleating properties of aerosol emitted from a range of industrial sites and processes. This should not be limited to a better understanding of the activity of candidate aerosol types in a pure form, but needs to take into account the chemical and physical environment that the particles are emitted in. For example, studies of ice nucleation by volcanic ashes show that their ice nucleating ability is strongly altered (enhanced or deactivated) by chemistry that occurs with reactive gases in the eruption plume and cloud (*42*, *48*). In addition, in order to assess the relative role of different INP types in these plumes as well as the wider atmosphere, we need to understand the size distribution of the aerosol types that are emitted. We typically characterise the ice nucleating activity of a material on an active site per surface area basis. Then with knowledge of the aerosol surface area, we can use the active site density to predict the INP concentration (as a function of activation temperature). This is important since the threshold temperature at which significant ice nucleation is observed in the atmosphere is strongly dependent on the available surface area and laboratory-derived threshold temperatures should therefore not be used as an indication of the temperature at which glaciation occurs in clouds.

Possible impacts of ice nucleating particles on clouds

Anthropogenic glaciation of supercooled liquid-water clouds downwind of industrial aerosol hot spots influences cloud cover and radiative fluxes. This is evident from the comparison between the properties of glaciation-affected areas downwind of air pollution hot spots and the properties of the nearby unaffected areas with supercooled liquid-water clouds based on MODIS satellite data (supplementary methods "Analysis of MODIS satellite data for selected aerosol sources;" Fig 2, Fig S14). We hand-logged the plume-shaped glaciation events at five aerosol sources: a copper smelter in Rouyn-Noranda, Canada; an oil refinery in Regina, Canada; a metallurgical plant in Cherepovets, Russia; and cement plants in Fokino and Volsk, Russia. At the time of the Terra MODIS overpass, the reflection of solar radiation to space at 0.545 to 0.565 μm is reduced by 13.7% (±0.7%) in the glaciation-affected areas owing to an 8.3% (±0.8%) reduction in cloud cover and an 18.0% (±3.5%) reduction in cloud optical thickness. At the same time, infrared radiance at 10.78 to 11.28 μm is enhanced by 4.2% (±0.2%) in the glaciation-affected areas, compared to nearby unaffected areas. In addition to glaciation-induced changes in the properties of clouds, the glaciation-induced snow on the ground could also influence radiative fluxes.

The anthropogenic glaciation events identified in this study could be the observable symptoms of the impact of anthropogenic INPs on clouds, in the same way as ship and pollution tracks in liquid clouds reveal the ability of anthropogenic aerosols serving as CCN to perturb liquid clouds (*26*). There is considerable monthly variability in the occurrence of glaciation events, with more cases in cold halfyear (Fig S12). Based on the visual signatures of glaciation events identified in Terra MODIS satellite images, we estimate that the probability of occurrence of glaciation events when susceptible supercooled liquid-water cloud decks occur ranges from 3.3% to 21.1% in cold half-year, with a high sensitivity to the screening of favourable conditions and studied pollution source (Fig 2c; supplementary methods "Meteorological conditions favourable for glaciation events;" Figs S15 and S16). It is also important to consider that visible anthropogenic cloud perturbations occur only at a subset of meteorological conditions and a plume might not be an analogue for a diffuse aerosol distribution, which then introduces sampling biases (*49*).

Further research is needed to understand glaciation events downwind industrial aerosol hot spots. Rare glaciation events downwind of nuclear power plants suggest that factors other than INPs may play a role in the glaciation events. Alternatively, buoyant plumes at nuclear power plants may loft nearby INPs. Moreover, further research is needed to quantify the ability of anthropogenic aerosols to serve as INPs, to quantify their impact on clouds, and to clarify if anthropogenic INPs influence Earth's climate.

References and Notes

1. P. Forster, T. Storelvmo, K. Armour, W. Collins, J.-L. Dufresne, D. Frame, D.J. Lunt, T. Mauritsen, M.D. Palmer, M. Watanabe, M. Wild, H. Zhang, 2021: The Earth's Energy Budget, Climate Feedbacks, and Climate Sensitivity. In *Climate Change 2021 – The Physical Science Basis: Working Group I Contribution to the Sixth Assessment Report of the Intergovernmental Panel on Climate Change* (Cambridge University Press, ed. 1, 2023; https://www.cambridge.org/core/product/identifier/9781009157896/type/book).
2. N. Bellouin, J. Quaas, E. Gryspeerdt, S. Kinne, P. Stier, D. Watson-Parris, O. Boucher, K. S. Carslaw, M. Christensen, A. -L. Daniau, J. -L. Dufresne, G. Feingold, S. Fiedler, P. Forster, A. Gettelman, J. M. Haywood, U. Lohmann, F. Malavelle, T. Mauritsen, D. T. McCoy, G. Myhre, J. Mülmenstädt, D. Neubauer, A. Possner, M. Rugenstein, Y. Sato, M. Schulz, S. E. Schwartz, O. Sourdeval, T. Storelvmo, V. Toll, D. Winker, B. Stevens, Bounding global aerosol radiative forcing of climate change. *Reviews of Geophysics* **58**(1), e2019RG000660 (2020).
3. B. J. Murray, D. O'Sullivan, J. D. Atkinson, M. E. Webb, Ice nucleation by particles immersed in supercooled cloud droplets. *Chem. Soc. Rev.* **41**, 6519 (2012).
4. P. J. DeMott, A. J. Prenni, X. Liu, S. M. Kreidenweis, M. D. Petters, C. H. Twohy, M. S. Richardson, T. Eidhammer, D. C. Rogers, Predicting global atmospheric ice nuclei distributions and their impacts on climate. *Proc. Natl. Acad. Sci. U.S.A.* **107**, 11217–11222 (2010).
5. S. M. Burrows, C. S. McCluskey, G. Cornwell, I. Steinke, K. Zhang, B. Zhao, M. Zawadowicz, A. Raman, G. Kulkarni, S. China, A. Zelenyuk, P. J. DeMott, Ice-nucleating particles that impact clouds and climate: Observational and modeling research needs. *Reviews of Geophysics* **60**(2), e2021RG000745 (2022).
6. U. Lohmann, A glaciation indirect aerosol effect caused by soot aerosols. *Geophys. Res. Lett.* **29**, 1052 (2002).
7. T. Storelvmo, J. E. Kristjánsson, U. Lohmann, Aerosol Influence on Mixed-Phase Clouds in CAM-Oslo. *J. Atmos. Sci.* **65**, 3214–3230 (2008).
8. A. Gettelman, X. Liu, D. Barahona, U. Lohmann, C. Chen, Climate impacts of ice nucleation, *Journal of Geophysical Research: Atmospheres*. **117** (2012).
9. M. P. Adams, M. D. Tarn, A. Sanchez-Marroquin, G. C. E. Porter, D. O'Sullivan, A. D. Harrison, Z. Cui, J. Vergara-Temprado, F. Carotenuto, M. A. Holden, M. I. Daily, T. F. Whale, S. N. F. Sikora, I. T. Burke, J. -U. Shim, J. B. McQuaid, B. J. Murray, A major combustion aerosol event had a negligible impact on the atmospheric ice-nucleating particle population. *JGR Atmospheres*. **125**(22), e2020JD032938 (2020).

10. Z. A. Kanji, A. Welti, J. C. Corbin, A. A. Mensah, Black carbon particles do not matter for immersion mode ice nucleation. *Geophysical Research Letters.* **47**(11), e2019GL086764 (2020).

11. J. Vergara-Temprado, M. A. Holden, T. R. Orton, D. O'Sullivan, N. S. Umo, J. Browse, C. Reddington, M. T. Baeza-Romero, J. M. Jones, A. Lea-Langton, A. Williams, K. S. Carslaw, B. J. Murray, Is Black Carbon an Unimportant Ice-Nucleating Particle in Mixed-Phase Clouds? *JGR Atmospheres*. **123**, 4273–4283 (2018).

12. F. Mahrt, C. Marcolli, R. O. David, P. Grönquist, E. J. Barthazy Meier, U. Lohmann, Z. A. Kanji, Ice nucleation abilities of soot particles determined with the Horizontal Ice Nucleation Chamber. *Atmos. Chem. Phys.* **18**, 13363–13392 (2018).

13. J. Chen, Z. Wu, S. Augustin-Bauditz, S. Grawe, M. Hartmann, X. Pei, Z. Liu, D. Ji, H. Wex, Ice-nucleating particle concentrations unaffected by urban air pollution in Beijing, China. *Atmos. Chem. Phys.* **18**, 3523–3539 (2018).

14. N. S. Umo, B. J. Murray, M. T. Baeza-Romero, J. M. Jones, A. R. Lea-Langton, T. L. Malkin, D. O'Sullivan, L. Neve, J. M. C. Plane, A. Williams, Ice nucleation by combustion ash particles at conditions relevant to mixed-phase clouds. *Atmos. Chem. Phys.* **15**, 5195–5210 (2015).

15. K. Bi, G. R. McMeeking, D. P. Ding, E. J. T. Levin, P. J. DeMott, D. L. Zhao, F. Wang, Q. Liu, P. Tian, X. C. Ma, Y. B. Chen, M. Y. Huang, H. L. Zhang, T. D. Gordon, P. Chen, Measurements of Ice Nucleating Particles in Beijing, China. *JGR Atmospheres*. **124**, 8065–8075 (2019).

16. M. Hartmann, T. Blunier, S. O. Brügger, J. Schmale, M. Schwikowski, A. Vogel, H. Wex, F. Stratmann, Variation of Ice Nucleating Particles in the European Arctic Over the Last Centuries. *Geophysical Research Letters*. **46**, 4007–4016 (2019).

17. C. R. Wood, R. G. Harrison, Anthropogenic snowfall events in the UK: examples of urban weather modification? *Weather*. **64**, 277–280 (2009).

18. M. L. Kramer, D. E. Seymour, M. E. Smith, R. W. Reeves, T. T. Frankenberg, Snowfall Observations from Natural-Draft Cooling Tower Plumes. *Science*. **193**, 1239–1241 (1976).

19. W. M. Culkowski, WEATHER NOTE: AN ANOMALOUS SNOW AT OAK RIDGE, TENNESSEE. *Mon. Wea. Rev.* **90**, 194–196 (1962).

20. F. P. Parungo, P. A. Allee, H. K. Weickmann, Snowfall induced by a power plant plume. *Geophysical Research Letters*. **5**, 515–517 (1978).

21. E. M. Agee, An Artificially Induced Local Snowfall. *Bull. Amer. Meteor. Soc.* **52**, 557–560 (1971).

22. B. Campistron, Interaction between a natural snowfall and a cooling tower plume: An experimental study with a millimetric Doppler radar. *Atmospheric Environment (1967)*. **21**, 1375–1383 (1967).

23. T. Storelvmo, I. Tan, The Wegener-Bergeron-Findeisen process – Its discovery and vital importance for weather and climate, *Meteorologische Zeitschrift*. **24**, 455–461 (2015).

24. S. Platnick, M. D. King, K.G. Meyer, G. Wind, N. Amarasinghe, B. Marchant, G. T. Arnold, Z. Zhang, P. A. Hubanks, B. Ridgway, J. Riedi, MODIS cloud optical properties: User guide for the Collection 6 Level-2 MOD06/MYD06 product and associated Level-3 Datasets. Version 1, 145 (2015).

25. V. Toll, M. Christensen, S. Gassó, N. Bellouin, Volcano and Ship Tracks Indicate Excessive Aerosol-Induced Cloud Water Increases in a Climate Model. *Geophysical Research Letters*. **44** (2017), doi:10.1002/2017GL075280.

26. V. Toll, M. Christensen, J. Quaas, N. Bellouin, Weak average liquid-cloud-water response to anthropogenic aerosols. *Nature*. **572**, 51–55 (2019).

27. J. Rahu, H. Trofimov, P. Post, V. Toll, Diurnal evolution of cloud water responses to aerosols. *JGR Atmospheres*. **127**(10), e2021JD035091 (2022).

28. H. Trofimov, P. Post, E. Gryspeerdt, V. Toll, Meteorological conditions favorable for strong anthropogenic aerosol impacts on clouds. *JGR Atmospheres*, **127**(4), e2021JD035871 (2022).

29. V. Toll, J. Rahu, Strong Anthropogenic Cloud Perturbations Can Persist for Multiple Days. *JGR Atmospheres*, **128**(9), e2022JD038146 (2023).

30. A. J. Heymsfield, G. Thompson, H. Morrison, A. Bansemer, R. M. Rasmussen, P. Minnis, Z. Wang, D. Zhang, Formation and Spread of Aircraft-Induced Holes in Clouds. *Science*. **333**, 77–81 (2011).

31. A. J. Heymsfield, P. C. Kennedy, S. Massie, C. Schmitt, Z. Wang, S. Haimov, A. Rangno, Aircraft-Induced Hole Punch and Canal Clouds: Inadvertent Cloud Seeding. *Bull. Amer. Meteor. Soc.* **91**, 753–766 (2010).

32. R. R. Draxler, G. D. Hess, An overview of the HYSPLIT_4 modelling system for trajectories. *Australian meteorological magazine*, **47**(4), 295-308 (1998).

33. J. Bühl, P. Seifert, R. Engelmann, A. Ansmann, Impact of vertical air motions on ice formation rate in mixed-phase cloud layers. *npj Clim Atmos Sci*. **2**, 36 (2019).

34. D. J. Cziczo, K. D. Froyd, C. Hoose, E. J. Jensen, M. Diao, M. A. Zondlo, J. B. Smith, C. H. Twohy, D. M. Murphy, Clarifying the Dominant Sources and Mechanisms of Cirrus Cloud Formation. *Science*. **340**, 1320–1324 (2013).

35. D. J. Cziczo, O. Stetzer, A. Worringen, M. Ebert, S. Weinbruch, M. Kamphus, S. J. Gallavardin, J. Curtius, S. Borrmann, K. D. Froyd, S. Mertes, O. Möhler, U. Lohmann, Inadvertent climate modification due to anthropogenic lead. *Nature Geosci*. **2**, 333–336 (2009).

36. M. S. Richardson, P. J. DeMott, S. M. Kreidenweis, D. J. Cziczo, E. J. Dunlea, J. L. Jimenez, D. S. Thomson, L. L. Ashbaugh, R. D. Borys, D. L. Westphal, G. S. Casuccio, T. L. Lersch, Measurements of heterogeneous ice nuclei in the western United States in springtime and their relation to aerosol characteristics. *J. Geophys. Res.* **112**, D02209 (2007).

37. Z. A. Kanji, L. A. Ladino, H. Wex, Y. Boose, M. Burkert-Kohn, D. J. Cziczo, M. Krämer, Overview of ice nucleating particles. *Meteorological Monographs*. **58**, 1-1 (2017).

38. A. D. Harrison, T. F. Whale, M. A. Carpenter, M. A. Holden, L. Neve, D. O'Sullivan, J. Vergara Temprado, B. J. Murray, Not all feldspars are equal: a survey of ice nucleating properties across the feldspar group of minerals. *Atmos. Chem. Phys.* **16**, 10927–10940 (2016).

39. A. D. Harrison, K. Lever, A. Sanchez-Marroquin, M. A. Holden, T. F. Whale, M. D. Tarn, J. B. McQuaid, B. J. Murray, The ice-nucleating ability of quartz immersed in water and its

atmospheric importance compared to K-feldspar. *Atmos. Chem. Phys.* **19**, 11343–11361 (2019).

40. J. D. Atkinson, B. J. Murray, M. T. Woodhouse, T. F. Whale, K. J. Baustian, K. S. Carslaw, S. Dobbie, D. O'Sullivan, T. L. Malkin, The importance of feldspar for ice nucleation by mineral dust in mixed-phase clouds. *Nature*. **498**, 355–358 (2013).

41. A. S. R. Murty, Bh. V. R. Murty, Ice nucleation by ordinary Portland cement. *Tellus*. **24**, 581–585 (1972).

42. E. C. Maters, C. Cimarelli, A. S. Casas, D. B. Dingwell, B. J. Murray, Volcanic ash ice-nucleating activity can be enhanced or depressed by ash-gas interaction in the eruption plume. *Earth and Planetary Science Letters*. **551**, 116587 (2020).

43. S. Grawe, S. Augustin-Bauditz, H.-C. Clemen, M. Ebert, S. Eriksen Hammer, J. Lubitz, N. Reicher, Y. Rudich, J. Schneider, R. Staacke, F. Stratmann, A. Welti, H. Wex, Coal fly ash: linking immersion freezing behavior and physicochemical particle properties. *Atmos. Chem. Phys.* **18**, 13903–13923 (2018).

44. N. Hiranuma, O. Möhler, K. Yamashita, T. Tajiri, A. Saito, A. Kiselev, N. Hoffmann, C. Hoose, E. Jantsch, T. Koop, M. Murakami, Ice nucleation by cellulose and its potential contribution to ice formation in clouds. *Nature Geosci*. **8**, 273–277 (2015).

45. N. Hiranuma, K. Adachi, D. M. Bell, F. Belosi, H. Beydoun, B. Bhaduri, H. Bingemer, C. Budke, H.-C. Clemen, F. Conen, K. M. Cory, J. Curtius, P. J. DeMott, O. Eppers, S. Grawe, S. Hartmann, N. Hoffmann, K. Höhler, E. Jantsch, A. Kiselev, T. Koop, G. Kulkarni, A. Mayer, M. Murakami, B. J. Murray, A. Nicosia, M. D. Petters, M. Piazza, M. Polen, N. Reicher, Y. Rudich, A. Saito, G. Santachiara, T. Schiebel, G. P. Schill, J. Schneider, L. Segev, E. Stopelli, R. C. Sullivan, K. Suski, M. Szakáll, T. Tajiri, H. Taylor, Y. Tobo, R. Ullrich, D. Weber, H. Wex, T. F. Whale, C. L. Whiteside, K. Yamashita, A. Zelenyuk, O. Möhler, A comprehensive characterisation of ice nucleation by three different types of cellulose particles immersed in water. *Atmos. Chem. Phys.* **19**, 4823–4849 (2019).

46. S. Bogler, N. Borduas-Dedekind, Lignin's ability to nucleate ice via immersion freezing and its stability towards physicochemical treatments and atmospheric processing. *Atmos. Chem. Phys.* **20**, 14509–14522 (2020).

47. Y. Mamane, J. L. Miller, T. G. Dzubay, Characterization of individual fly ash particles emitted from coal- and oil-fired power plants. *Atmospheric Environment (1967)*. **20**, 2125–2135 (1986).

48. W. D. Fahy, E. C. Maters, R. Giese Miranda, M. P. Adams, L. G. Jahn, R. C. Sullivan, B. J. Murray, Volcanic ash ice nucleation activity is variably reduced by aging in water and sulfuric acid: the effects of leaching, dissolution, and precipitation. *Environ. Sci.: Atmos.* **2**, 85–99 (2022).

49. P. Manshausen, D. Watson-Parris, M. W. Christensen, J.-P. Jalkanen, P. Stier, Invisible ship tracks show large cloud sensitivity to aerosol. *Nature*. **610**, 101–106 (2022).

50. V. V. Salomonson, W. Barnes, E. J. Masuoka, "Introduction to MODIS and an Overview of Associated Activities" in *Earth Science Satellite Remote Sensing*, J. J. Qu, W. Gao, M. Kafatos, R. E. Murphy, V. V. Salomonson, Eds. (Springer Berlin Heidelberg, Berlin, Heidelberg, 2006; http://link.springer.com/10.1007/978-3-540-37293-6_2), pp. 12–32.

51. T. J. Schmit, P. Griffith, M. M. Gunshor, J. M. Daniels, S. J. Goodman, W. J. Lebair, A Closer Look at the ABI on the GOES-R Series. *Bulletin of the American Meteorological Society*. **98**, 681–698 (2017).

52. I. M. Lensky, D. Rosenfeld, Clouds-Aerosols-Precipitation Satellite Analysis Tool (CAPSAT). *Atmos. Chem. Phys.* **8**, 6739–6753 (2008).

53. C. B. Elsenheimer, C. M. Gravelle, Introducing Lightning Threat Messaging Using the GOES-16 Day Cloud Phase Distinction RGB Composite. *Weather and Forecasting*. **34**, 1587–1600 (2019).

54. J. Reid, D. Hudak, S. Boodoo, N. Donaldson, P. Joe, D. Kiktev, A. Melnichuk, Dual-polarisation radar particle classification results during the Sochi Olympic Games. In Eighth European Conf. on Radar in Meteorology and Hydrology, Garmisch-Partenkirchen, Germany, DWD–DLR. [Available online at www. pa. op. dlr. de/erad2014/programme/ExtendedAbstracts/151_Reid. pdf.].

55. H. S. Park, A. V. Ryzhkov, D. S. Zrnić, K.-E. Kim, The Hydrometeor Classification Algorithm for the Polarimetric WSR-88D: Description and Application to an MCS. *Weather and Forecasting*. **24**, 730–748 (2009).

56. H. Hersbach, B. Bell, P. Berrisford, S. Hirahara, A. Horányi, J. Muñoz-Sabater, J. Nicolas, C. Peubey, R. Radu, D. Schepers, A. Simmons, C. Soci, S. Abdalla, X. Abellan, G. Balsamo, P. Bechtold, G. Biavati, J. Bidlot, M. Bonavita, G. De Chiara, P. Dahlgren, D. Dee, M. Diamantakis, R. Dragani, J. Flemming, R. Forbes, M. Fuentes, A. Geer, L. Haimberger, S. Healy, R. J. Hogan, E. Hólm, M. Janisková, S. Keeley, P. Laloyaux, P. Lopez, C. Lupu, G. Radnoti, P. De Rosnay, I. Rozum, F. Vamborg, S. Villaume, J. Thépaut, The ERA5 global reanalysis. *Quart J Royal Meteoro Soc*. **146**, 1999–2049 (2020).

Acknowledgments: We thank Robert Oscar David for the discussions on the ability of various types of anthropogenic aerosols to serve as ice-nucleating particles. We thank Dmitry Moiseev for pointing out previous research on anthropogenic snowfall events.

Funding:

Estonian Research Council grant PRG1726 (VT, JR, HK, HT, PP)

European Research Council (ERC) H2020 project RECAP with grant agreement 724602 (PS)

FORCeS project under the European Union's Horizon 2020 research program with grant agreement 821205 (PS, TS)

Atmospheric System Research (ASR) program of DOE BER under Pacific Northwest National Laboratory (PNNL) project 57131; PNNL is operated for DOE by the Battelle Memorial Institute under contract DE-A06-76RLO 1830 (MC)

GreenFeedBack Hop On project under the European Union's Horizon 2020 research program with grant agreement 101056921 (HJ, VT)

ACCC Flagship funded by the Academy of Finland grant number 337549 (MK)

Natural Environment Research Council (NERC) project NE/T00648X/1 (M-Phase) (BM)

European Union's Horizon 2020 research and innovation programme under Marie Skłodowska-Curie grant agreement No 860100 (iMIRACLI) (PM)

Author contributions: VT discovered the glaciation events and conceptualised and led the research. HK, HT, JR and VT analysed MODIS satellite observations. JR, PP and VT analysed GOES ABI satellite observations. JR, TV, EH, ND, DM and VT analysed precipitation radar data. PM and MC simulated aerosol dispersion. HK analysed meteorological reanalysis data. HK, JR and VT compiled figures. VT wrote the paper with contributions from all co-authors.

Competing interests: Authors declare that they have no competing interests.

Data and materials availability: We acknowledge the use of imagery from NASA's Worldview application (https://worldview.earthdata.nasa.gov), part of NASA's Earth Observing System Data and Information System (EOSDIS). MODIS data are freely available from https://ladsweb.modaps.eosdis.nasa.gov/search/. NOAA Geostationary Operational Environmental Satellites (GOES) ABI data was accessed from https://registry.opendata.aws/noaa-goes. ERA5 data are freely available from https://cds.climate.copernicus.eu/. The data and software used to analyse glaciation events will be available at https://datadoi.ee/handle/33/610 at the time of the publication and are available at Gitlab for now https://gitlab.cs.ut.ee/ut-climate-research-centre/ACI/glaciation-tracks-published.

Supplementary Materials

Materials and Methods

Figs. S1 to S16

References (*50–56*)

Movies S1 to S3

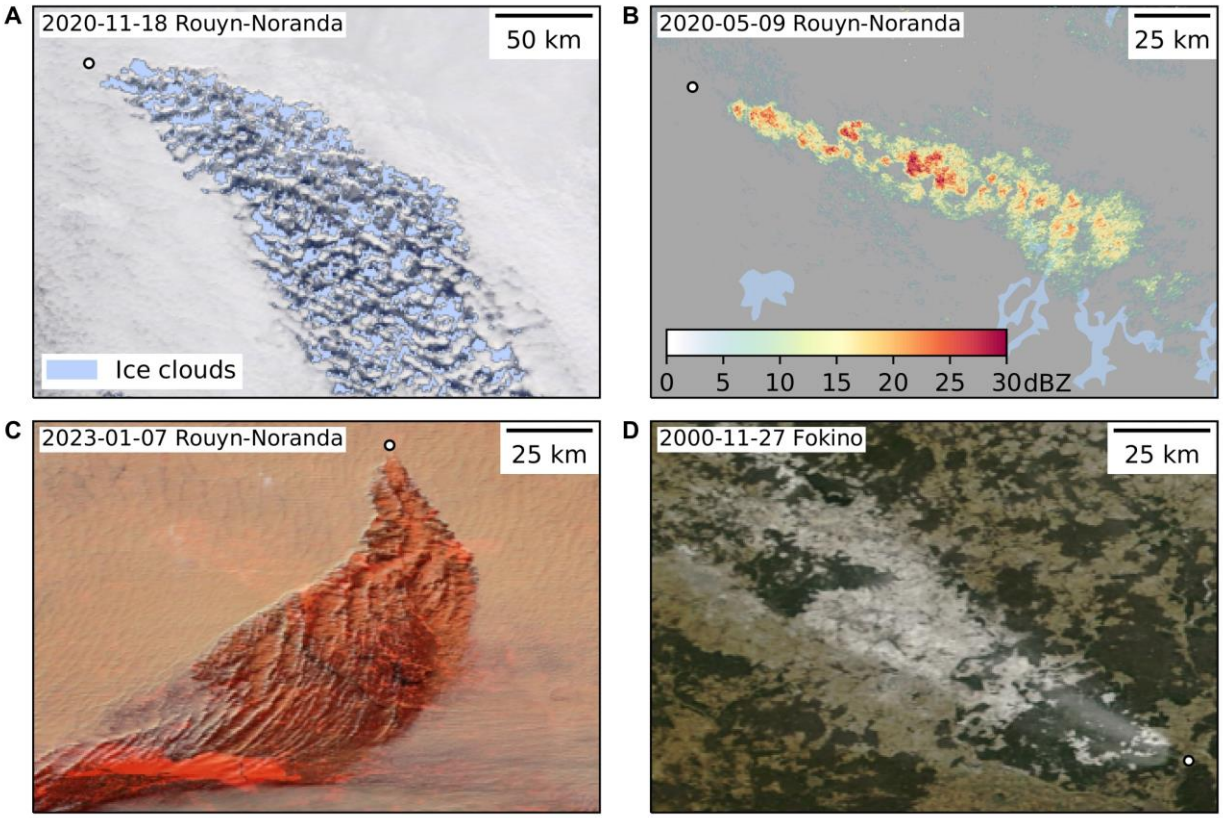

Fig. 1. Plume-shaped areas of anthropogenic glaciation of supercooled clouds, snowfall, reduced cloud cover and snow on the ground for different glaciation events. Remote sensing data reveals ice clouds in the middle of supercooled liquid clouds, snowfall and reduced cloud cover downwind of industrial air pollution hot spots. In all panels, the circle denotes the location of an air pollution source. (**A**) Glaciated area with ice clouds in the middle of supercooled liquid-water clouds downwind of the Copper smelter in Rouyn-Noranda, Canada, overlain on the MODIS daytime true colour satellite image on November 18th 2020. A plume of ice clouds, based on the MODIS cloud phase optical properties product, is highlighted in light blue colour and supercooled liquid clouds are depicted in grey-white colours, based on the true colour satellite image. (**B**) A plume of snow in ground-based precipitation radar reflectivity [dBZ] is shown in green-yellow-red colours downwind of the Copper smelter in Rouyn-Noranda, Canada on May 9th 2020. The ground-based radar is situated in Landrienne, i.e. 85 km northeast of the smelter. (**C**) Area of reduced cloud cover downwind of the Copper smelter in Rouyn-Noranda, Canada, in the MODIS daytime near-infrared composite satellite image on January 7th 2023. The supercooled liquid clouds are depicted in light brownish colours and the plume-shaped area of reduced cloud cover is depicted in darker brownish-red colours as ice and snow cover the ground. In addition, glaciated clouds are shown in red colours. (**D**) A plume-shaped area of snow on the ground downwind of the cement plant in Fokino, Russia, in the MODIS daytime true colour satellite image on November 27th 2000. Snow is depicted in grey-white colours and the ground in green colours. The plume-shaped area of snow on the ground became visible after the glaciation event when the cloud deck cleared away.

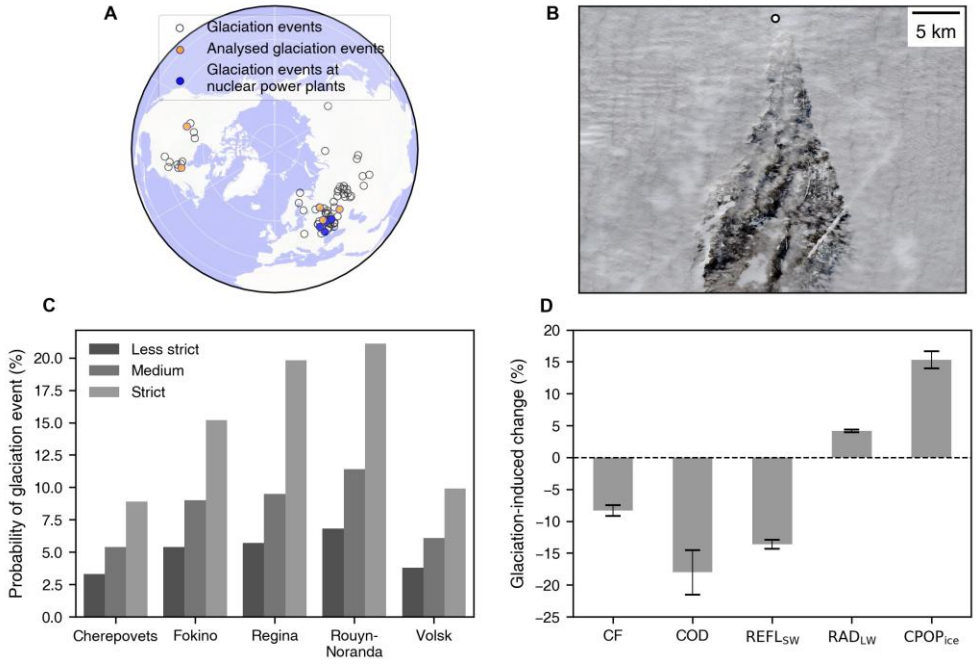

Fig. 2. Anthropogenic glaciation of supercooled liquid-water clouds impacts cloud properties and radiative fluxes. (**A**) Empty circles and orange dots mark the locations of anthropogenic aerosol hot spots where glaciation events have been identified. MODIS data in the years 2000 to 2021 is sampled for the locations given with the orange dots. Glaciation is also observed at nuclear power plants marked with blue dots. (**B**) In the true colour Sentinel-2 MultiSpectral Instrument daytime satellite image, the land surface is seen through the glaciation-induced hole in the supercooled liquid-water cloud deck downwind of the copper smelter in Rouyn-Noranda, Canada on January 9th 2021. The glaciation-affected area is darker compared to the nearby area covered by supercooled liquid-water clouds (depicted in grey-white colours) due to reduced back-scattering of solar radiation to space. The white circle denotes the location of the aerosol source. (**C**) Probability to identify glaciation event in Terra MODIS satellite image in cold half-year (October to March) in case supercooled liquid-water cloud decks susceptible to glaciation occur. The studied sites are a steel plant in Cherepovets, cement plants in Fokino and Volsk, an oil refinery in Regina and a copper smelter in Rouyn-Noranda. The probability depends on the strictness of the screening of favourable conditions (supplementary methods "Meteorological conditions favourable for glaciation events") as indicated by the hue. (**D**) Average fractional changes in cloud fraction (CF), cloud optical depth (COD), shortwave reflectance at 0.545 to 0.565 µm ($REFL_{SW}$), and longwave radiance at 10.78 to 11.28 µm (RAD_{LW}), and the average difference in the fraction of ice-phase pixels in the glaciation-affected areas based on Cloud Phase determined by the Optical Properties algorithm ($CPOP_{ice}$; *24*), compared to nearby unaffected areas based on MODIS data for 298 glaciation events, together with standard errors.

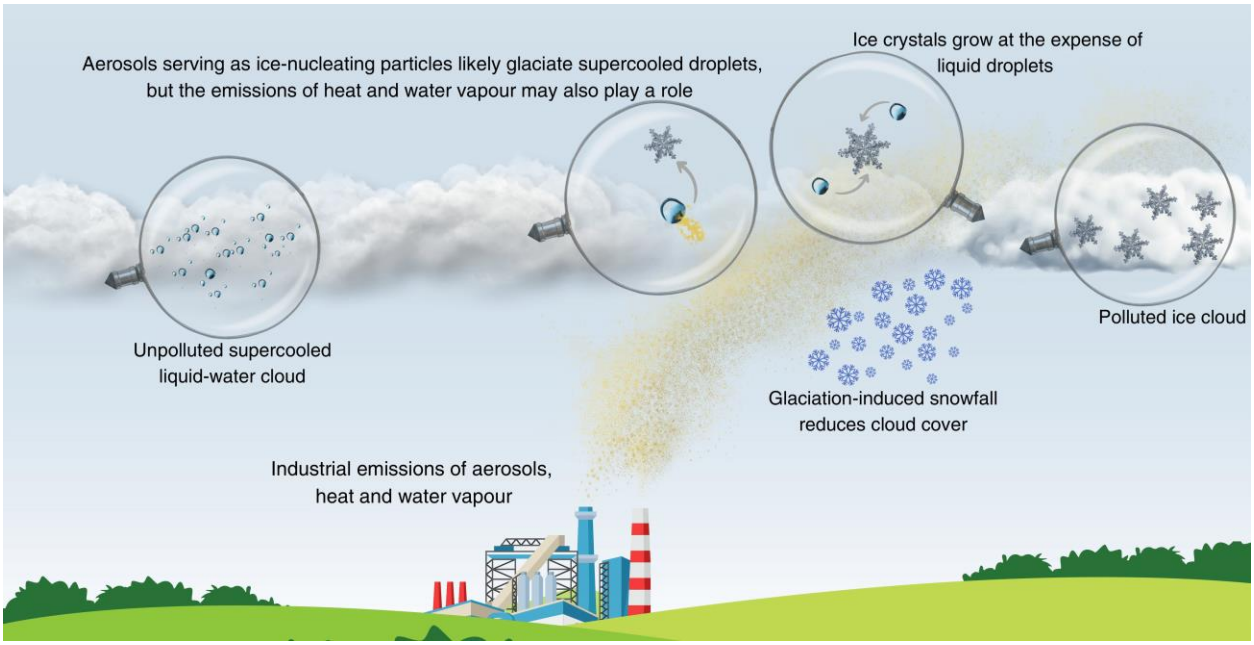

Fig. 3. Industrial emissions lead to the glaciation of supercooled clouds, snowfall and reduced cloud cover, while aerosols serving as ice-nucleating particles likely play a dominant role in the glaciation. Ice clouds in the middle of supercooled liquid-water clouds and snowfall are observed downwind of industries like metallurgical and cement factories. Anthropogenic aerosols serving as INPs likely transform supercooled cloud droplets into ice crystals at the studied air pollution hot spots, although the emissions of heat and water vapour may also play a role, as suggested by glaciation events downwind nuclear power plants. The ice crystals could subsequently grow at the expense of supercooled droplets. Finally, the growth of ice crystals leads to snowfall that reduces cloud cover.

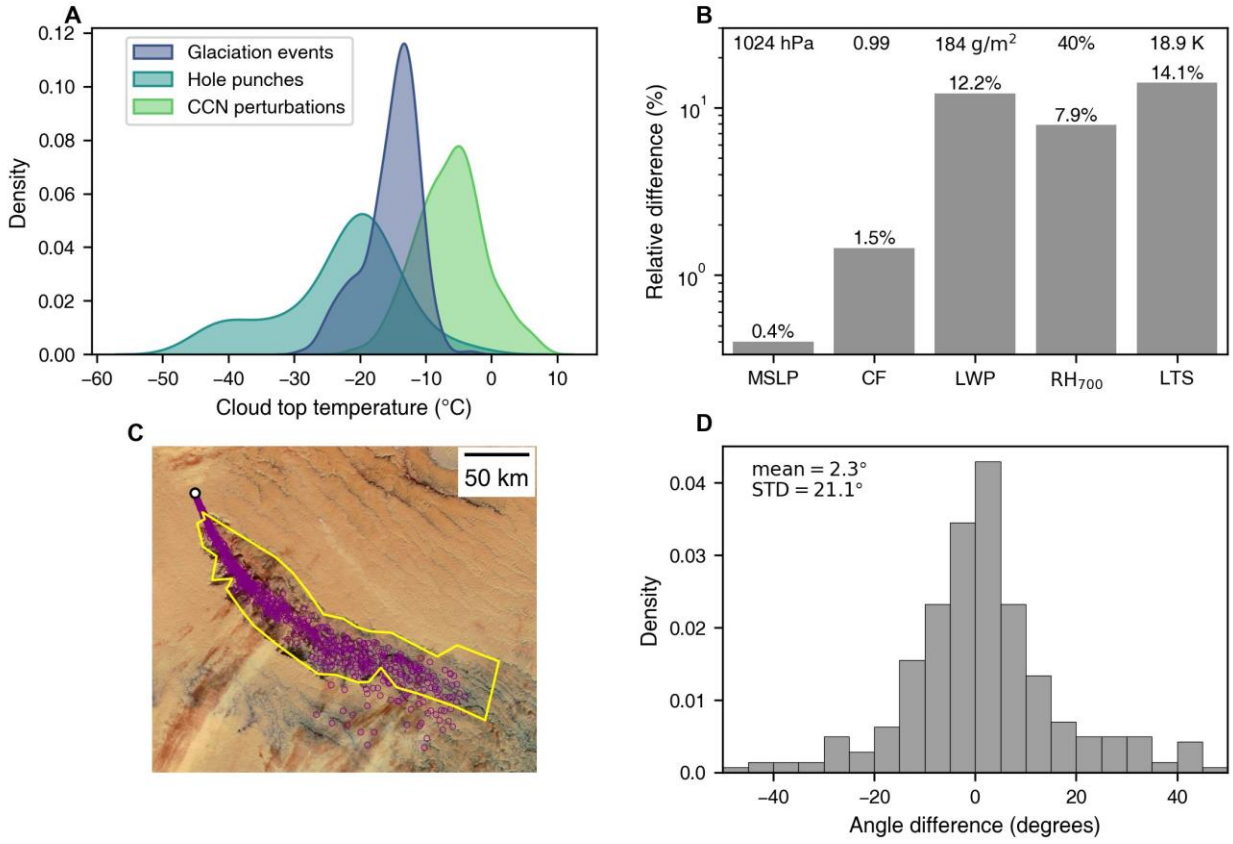

Fig. 4. Linking glaciation events to industrial emissions. (**A**) MODIS cloud top temperatures (°C). Glaciation events downwind aerosol hot spots occur at colder temperatures compared to cloud condensation nuclei (CCN) perturbations but at higher subzero temperatures compared to aircraft-induced hole punch clouds at Moscow Domodedovo airport. The temperatures for the Volsk cement plant in Russia are not shown, as we only identified glaciation events there. (**B**) The relative difference [%] of meteorological conditions characteristic of glaciation events from conditions characteristic of CCN perturbations. Average mean sea level pressure (MSLP), cloud fraction (CF), liquid water path (LWP), relative humidity at 700 hPa pressure level (RH700) and lower tropospheric stability (LTS) are compared. On the top of the panel, average conditions for glaciation events are given. The data for the Volsk cement plant in Russia are not shown, as we only identified glaciation events there. (**C**) MODIS daytime near-infrared composite satellite image of supercooled liquid-water clouds on November 18th 2006. The supercooled clouds are depicted in brownish colours. The yellow polygon surrounds the area of a glaciation event identified and hand-logged in satellite data. The glaciated area overlaps with the simulated aerosol-polluted area, given with violet dots, strikingly well. The white circle denotes the location of the aerosol source - the copper smelter in Rouyn-Noranda, Canada. (**D**) The differences in azimuths (degrees) between glaciation events identified in MODIS satellite data and simulated aerosol-polluted areas downwind of industrial aerosol sources are relatively small. The differences that are larger than 50 degrees are not shown.

Table 1. Emissions from metallurgy, processing of minerals, hydrocarbon combustion, paper production, and nuclear power plants lead to the glaciation of supercooled liquid-water clouds. For each emission source group, the count of identified emission sources leading to glaciation is given together with the list of identified emission source types.

Emission source group	List of emission sources	Count of identified emission sources leading to glaciation events
Metallurgy	Machine building, processing of steel, iron, copper, nickel, alumina	32
Minerals	Production of cement, asphalt, and mineral fertilisers	20
Hydrocarbon combustion	Coal-fired power plants, oil refineries, production of petrochemicals	12
Cellulose	Production of cellulose and paper	3
Low aerosol emission power plants	Nuclear power plants	4